Published in final edited form as:
NMR Biomed. 2012 February ; 25(2): 347–358. doi:10.1002/nbm.1756.

Real-time Motion and B0 correction for LASER MRSI using EPI volumetric navigators

Aaron T. Hess[1], **Ovidiu C. Andronesi**[2,3], **M. Dylan Tisdall**[2,3], **A. Gregory Sorensen**[2,3], **André J.W. van der Kouwe**[2,3], and **Ernesta M. Meintjes**[1]

[1]MRC/UCT Medical Imaging Research Unit, Department of Human Biology, University of Cape Town, South Africa

[2]Athinoula A. Martinos Center for Biomedical Imaging, MGH, Charlestown, MA

[3]Department of Radiology, Harvard Medical School, Boston, MA

Abstract

A method is presented to correct the effects of motion and motion-related B0 perturbations on spectroscopic imaging in real-time through the use of a volumetric navigator (vNav). It is demonstrated that for an axial slice, lifting the chin significantly disrupts the B0 homogeneity in the zero-order (frequency), first-order Y (coronal) axis, and in the second-order ZY term. This vNav is able to measure and correct in real time both head pose and zero- to first-order B0 inhomogeneities. The vNav has been validated in six volunteers who deliberately lifted and then dropped their chin during the scan. These scans show that motion correction alone is not enough to recover the spectral quality. By applying real-time shim adjustments, spectral quality was fully recovered to line widths under 0.08 ppm and SNR to within acceptable limits in five out of six subjects. In the sixth subject 83% of the spectra within the VOI were recovered, compared to the worst case non-shim corrected scan where none of the voxels fell within these quality bounds. It is shown that the use of a vNav comes at no additional cost to the scan time or spectral SNR.

Keywords

MRSI; spectroscopy; motion correction; shim correction; real-time; navigator

Abbreviations

vNav; MEMPR; PROMO; LASER; PACE; NAA; tCr; ShMoCo; MoCo; NoCo

Introduction

Magnetic resonance spectroscopic imaging (MRSI) is a powerful non-invasive tool for studying biochemistry *in vivo*. However, it suffers from a lack of anatomical resolution and is sensitive to temporal fluctuations in the B0 magnetic field. By contrast to MR imaging, motion during MRSI does not always cause observable artefacts and image displacement and as such may go completely unnoticed. Some of the more observable motion-related artefacts in MRSI include lipid contamination, ghosting, and line broadening. The former occurs when the subject's movement causes the volume of interest (VOI) to intersect with a lipid containing region, potentially rendering a large proportion of the spectra unusable.

Contact details: Aaron T. Hess, hess.aaron@gmail.com, fax: + 27 21 448 7226, mobile: +44 7806 387578, OCMR, John Radcliffe Hospital, Headington, Oxford, OX3 9DU, United Kingdom.

Free-induction decay (FID) dephasing caused by rapid movements by the subject during application of the outer-volume suppression gradients will manifest as ghosting artefacts and amplitude fluctuations. Split spectral peaks and line broadening result from changes in the B0 field due to the new orientation of susceptibility boundaries. Finally, changes in proximity to various coil elements will cause spatially related phase changes in the received signal.

There are various degrees of B0 adjustment in clinical systems ranging from zero-order (frequency) to second- or even third-order spatial adjustments. Several methods have been proposed to prospectively and retrospectively track the *in vivo* zero-order B0 field. One such method initiates the FID readout prior to the application of phase encoding gradients (1). In this manner, the non-encoded portion of the FID can be used for phase and frequency correction. An alternative method uses an interleaved navigator with a 5° excitation followed by an FID readout (2) to measure the change of the main magnetic field frequency. Tracking of the mean VOI frequency can be achieved if outer-volume suppression is added (3). None of these methods address first- or higher-order B0 changes.

Several real-time head tracking methods have been used in MRI including optical tracking devices and within-sequence navigator methods. Optical tracking devices (4,5) use an externally mounted camera to track the subject's movement. One advantage of such systems is a unified coordinate system for both anatomical imaging and spectroscopic imaging, thus providing confidence in MRSI VOI placement and the fact that sequences do not need to be changed fundamentally. The main disadvantage of such devices is the cumbersome additional hardware in the MR room and additional regalia worn by the subject. Navigator methods, on the other hand, require no additional hardware.

Navigator-based motion tracking can be performed using the properties of rigid body transformations exhibited in rapid k-space trajectories. Examples of these are cloverleaf (6) and orbital (7) navigators that can be executed in under 10 ms. An alternative is to use image based navigator techniques such as the EPI volumetric Navigator (vNav) (8,9). The vNav method employs 3D multi-shot EPI to rapidly generate a low resolution 3D image of the subject and register it to a reference volume. A technique that employs three orthogonal low resolution 2D spiral images and registers these to a map has been proposed (10) and is called PROspective MOtion correction or PROMO. The vNav is particularly suited to MRSI as it performs well in sequences with low temporal resolution (long repetition times) and, with respect to MRSI, is the only technique capable of performing real-time first-order shim correction. In MRSI, TR's are of the order of 1.5 s to 3 s. In addition, the vNav provides a crude anatomical image which has the potential for registration to a structural image. Finally, it can generate spatial parameters such as a 3D B0 field map (9) that can be used to measure shim adjustment terms.

To establish the need for a real-time B0 corrected sequence with real-time VOI position and orientation correction, the B0 distortions resulting from motion were quantified in a single volunteer. This was done by acquiring high resolution B0 field maps for both chin left-to-right and chin down-to-up movements. A navigated Localized Adiabatic SElective Refocusing (LASER) (11) MRSI sequence is presented. The sequence uses an EPI vNav to measure and correct, in real time, VOI position, frequency and first-order shim changes. Six volunteers were scanned to demonstrate how real-time zero- to first-order B0 correction recovers the spectra in the presence of chin-up or -down rotations. Using the zero- to second-order B0 terms measured by the vNav we plot the B0 changes that accompany this motion for one of the volunteers.

Materials and Methods

Two scanners were used in this study: a 3T Siemens Allegra scanner (Erlangen, Germany) in Cape Town, South Africa using a standard single channel head coil; and a Siemens 3T Tim Trio at the Martinos Center, Boston, Massachusetts, with a standard 12 channel head coil. All volunteers were scanned according to the ethical guidelines of the respective institution.

Analysis of B0 change with respect to pose

To determine the role of frequency, first-order, and second-order shim correction in motion corrected MRSI, the effect of head movement on B0 homogeneity was investigated. We acquired multiple high-resolution B0 field maps in a single volunteer with the subject's head in various positions. The 3T Allegra scanner was used for the experiment. The volunteer was instructed to move their head incrementally, first about the X axis (chin down-to-up) and then about the Z axis (left-to-right rotation). Six field maps were acquired during the X axis rotation, ranging from 7.2° to −14.4°, and 6 field maps for the Z axis rotation, ranging from −19° to 16°. The subject was trained how much to move his head prior to scanning with resultant rotations assessed offline.

A gradient echo sequence was used to acquire the field maps. The parameters were as follows: 48 slices, matrix 64 × 64, FOV = 192 × 192 mm^2, slice thickness = 3 mm, TR = 502 ms, TE_1 = 4.59 ms, TE_2 = 7.05 ms, bandwidth = 260 Hz/pixel and a slice separation of 0.6 mm. No shim adjustment was performed prior to each field map acquisition.

Each field map was registered to a reference 3D Multi echo MPRAGE (MEMPR) (12) using SPM5 (13) in order to remove the effect of shifting anatomy, and further resliced to match the 3D MEMPR resolution of 1.0 × 1.3 × 1.0 mm^3 using linear interpolation. An axial VOI was selected superior to the ventricles. For both movement trajectories, one position was taken as the neutral head pose. In the chin down-to-up trajectory, this was the third position and in the chin left-to-right trajectory this was the fourth position. To remove the effect of B0 inhomogeneities that would normally be corrected by the scanner's automated shimming procedure, a VOI-specific second-order shim estimate was calculated for each of the two neutral poses. This shim estimate was then subtracted from each field map in the respective series to emulate the expected B0 field in a shimmed MRSI experiment. Two operations were performed on the acquired field maps, firstly a mean frequency was calculated within the VOI. Secondly a 1 × 1 × 1.5 cm^3 kernel was convolved with the field maps to emulate the resolution, and thus mean frequency of an MRSI voxel.

LASER sequence with vNav for real-time shim and motion correction

A dual-contrast multi-shot 3D EPI vNav (9) was inserted into a LASER MRSI sequence (11), where *f* in equation 9 in reference (11) was set equal to zero. The vNav calculates both shim and head pose once per TR and applies the relevant corrections within the same TR. It has been shown that this LASER sequence has excellent spatial and chemical shift localisation (11).

The vNav EPI protocol used is as follows: 32 × 32 matrix, 16 slices, 256 × 256 × 128 mm^3 FOV (8 × 8 × 8 mm^3 isotropic). Two contrasts were generated with interleaved partition acquisitions: TE_1 = 6.6 ms and TE_2 = 9.0 ms, TR = 16 ms, and bandwidth = 3906 Hz/px. The two volumes were acquired interleaved in 34 shots, each with a 2° flip angle. The first two shots acquire the phase correction navigator used for N/2 ghost reduction of the two contrasts and the remaining 32 shots acquire 16 partition encodes, interleaved, for each contrast, giving a total navigator duration of 544 ms. The navigator is positioned over the

subject's brain using a "set" sequence that runs a single repetition of the navigator in the chosen position and is completed in under 1 s.

The vNavs are reconstructed immediately online and a field map is generated from the complex division of the two EPI volumes. Pose estimation is performed using a single vNav contrast (TE_1) by coregistering subsequent vNav's to the first vNav after the preparation ("dummy") TR's. This registration is performed using an optimised Prospective Acquisition CorEction (PACE) (14) algorithm that is an established method for registering whole-head EPI. The image reconstruction and PACE registration is performed online immediately after the navigator block in under 80 ms.

A mask is created to exclude voxels with an insufficient signal to noise ratio (SNR). The mask is defined as all voxels with a magnitude greater than max(|all voxels|)/15. This threshold was empirically determined to optimally exclude background noise without excluding brain voxels. Field map phase unwrapping is then performed online using PRELUDE (15). Two pairs of frequency and first-order shim estimates are calculated online, one for the required MRSI VOI and one for the navigator FOV. The shim estimates for the navigator FOV are calculated using an unweighted least squares regression while the shim estimate for the chosen VOI uses a weighted least squares regression, where the weighting of each navigator voxel is according to its intersection with the MRSI VOI. The final two adjustments performed during shim estimation are, firstly, to correct for the B0 distortion of each voxel (16) and, secondly, to shift the VOI according to the motion estimate for the current TR. This ensures that the voxel coordinates are mapped to the scanner coordinates taking into account the current pose. Hence shim estimation can only be performed after completion of PACE. The complete online block, including transmission of the current estimates back to the sequence, occurs in less than 170 ms, enabling the sequence to update the spectroscopy VOI according to current pose and apply the appropriate shim estimate to that VOI within the same TR. The total navigator block, including sequence (544 ms) and online processing (170 ms) takes 714 ms.

The MRSI LASER sequence was set up with the following parameters: TE = 50 ms, TR = 1500 ms, elliptical phase encoding (16×16 matrix), FOV = 208 × 224 mm^2, a Hamming filter applied that affects all data points in the outer half (50%) of k-space, 1 acquisition, TA = 3 min 50 s, final matrix size 32×32. Offset independent adiabatic pulses (T_p = 4 ms, BW = 6 kHz) based on WURST-8 waveforms (11,17) were used for selection of VOI (80 × 90 × 15 mm^3, APxRLxFH). Constant gradients were enforced to enable dynamic slice positioning using a frequency offset. Water suppression was realized with a WET scheme (18). Outer volume suppression (OVS) was not necessary due to the sharp LASER excitation profile of the VOI.

The vNav was inserted into the LASER sequence prior to water suppression, occupying a portion of the TR used for M0 relaxation. It has been shown that in SVS the small flip angle of the vNav does not observably affect the M0 relaxation process (9). The navigator real-time shim estimates are applied from the first preparation TR while the pose estimates are applied from the second TR after preparation. The navigator additionally calculates a VOI specific second-order B0 shim that is not applied, but recorded in a log file.

Validation of navigated LASER sequence

The sequence was validated in six healthy volunteers; two were scanned at the Martinos Center on a 3T Siemens Tim Trio (Erlangen, Germany) using a standard 12 channel head coil, and four at the Cape Universities Brain Imaging Centre on a 3T Siemens Allegra (Erlangen, Germany) using a standard single channel head coil. The protocol consisted of a structural MEMPR used for VOI localisation, followed by five vNav LASER MRSI scans

with an 80 × 90 × 15 mm^3 VOI positioned axially above the ventricles. The pre-scan shim was adjusted automatically by the scanner over the MRSI VOI. For scans at the Martinos Center, 256 FID samples were acquired per readout and in Cape Town, 512 FID samples were acquired per readout, both at a bandwidth of 1024 Hz. While the 512 FID samples will provide an increased spectral resolution for the scans in Cape Town, the 12 channel head coil used at the Martinos Center will increase SNR for those scans. These inter site differences will not have an impact on the data as only intra-subject comparisons of scans are presented.

For the first two MRSI scans the volunteers were asked not to move. In the first scan, real-time shim and motion correction (ShMoCo) were applied, and in the second the navigated sequence was used with the feedback disabled i.e. no correction applied (NoCo). For the remaining three scans the volunteers were trained to lift their chin by approximately 5°–10° on a cue presented 1 min into the scan, drop it approximately 5° lower than the neutral position after a further 1 min 15 s, and hold it there for the remainder of the scan (a further 1 min 35 s). After each scan they returned to the neutral position. One scan was acquired with shim and motion correction applied (ShMoCo), one with only motion correction applied (MoCo), and one with no correction applied (NoCo). These scans were executed in random order.

The spectra were processed in LCModel (19) using standard approaches with a LASER sequence-specific basis set. Two SNR measures were calculated. The first (SNR_{LCM}) is the SNR reported by LCModel. SNR_{LCM} is defined as the spectral maximum divided by two times the RMS of the residual. An additional measure of SNR (SNR_{NAA}) was calculated as the maximum of the N-Acetylaspartate (NAA) peak (between 1.9 and 2.2 ppm) divided by the standard deviation of the signal between 0.5 and 0.2 ppm. When computing SNR_{NAA} we used the raw spectra after LCModel phase and baseline correction in order to remove the effect of baseline distortions which were particularly prevalent when no shim correction was used.

Two further volunteers were scanned, volunteer 7 and 8, on the Siemens 3T Allegra scanner in Cape Town. Volunteer 7 was scanned to confirm that the vNav has no observable effect on the spectral SNR. This was previously shown in single voxel spectroscopy (9). The volunteer was scanned three times while they remained stationary. The first scan was acquired using the standard LASER sequence, while the second and the third were acquired with the navigated LASER sequence. The second was acquired with shim and motion correction applied (ShMoCo) and the third with no correction applied (NoCo). In this manner the effect on spectral quality of the vNav and applying the correction can be determined separately.

Volunteer 8 was scanned in order to investigate the performance of the navigated sequence with pseudo random movements. The subject was scanned three times, first with the standard LASER sequence while the subject remained stationary. In the second and third scans the navigated LASER sequence was used and the subject was asked to perform a random cycle of motions that they could repeat throughout the duration of the scan. The subject moved upon an audible cue every 11 s to 12 s. The first of these two scans with motion was acquired with ShMoCo, while the second was acquired with NoCo. The resultant motion trajectories were assessed offline to ensure that the pattern of motion in these two scans was comparable.

Results

Analysis of B0 change with respect to pose

The processed field maps acquired in a single volunteer are shown in Figure 1. This figure shows i) the pose-to-pose mean VOI-frequency and ii) a frequency difference map of the higher-order B0 changes, calculated by subtracting the mean VOI-frequency and the frequency map from the neutral head position. Significant frequency, first- and higher-order changes are evident in the chin-up and –down poses. In the chin-left and chin-right poses only small frequency changes are evident. In the two extreme chin-left positions (−12° and −19°), nonzero-order effects are evident at the edge of the VOI with roughly a 5 Hz – 10 Hz amplitude.

Validation of navigated LASER sequence

Figure 2 is an example of the first contrast of a single vNav acquisition and the phase unwrapped field map from both echoes.

The frequency, first-order, and second-order shim was measured by the vNav during each scan acquired with the navigated laser sequence in the six volunteers who performed a chin-up to chin-down movement. As an example, the motion and shim logged by the vNav for the ShMoCo scan of one of the volunteers are plotted in Figure 3. The motion measurements have been transformed into the same coordinate system as the scanner's shim gradients (scanner XYZ coordinate system). In Figure 3b we plot the mean frequency within the VOI. The frequency was calculated from the sum of the mean VOI frequency and the frequency offset resulting from the applied first-order shim. Figure 3c shows the first-order shim estimate, scaled to Hz/cm. This scale facilitates an interpretation of the expected frequency shifts across the VOI as a result of the change. Figure 3d shows the second-order shim change scaled to Hz/cm^2. Figure 3 demonstrates the variance in the vNav measurements. In most of the scans the Z^2 shim estimate was very noisy, varying by as much as 3 Hz/cm^2 in some volunteers. The variance of the motion estimates was consistent between volunteers with worst case standard deviations during a stationary scan of ±0.6 mm and ±0.6°.

Figure 4 is a series of scatter plots demonstrating intersubject zero- to second-order shim changes, as determined by the vNav, as a function of the angle of rotation of the head about the sagittal (X) axis. For the first-order plots, the X shim was excluded as it did not demonstrate a significant shim change in any of the volunteers. For the same reason, only YZ and Z^2 are plotted for the second-order changes. Only volunteer 4 demonstrated a change in $X^2 - Y^2$ of 0.17 Hz/cm^2. Data from volunteers 1 and 2 were not included in the second-order scatter plots as second-order shim logs were not recorded during these scans.

Figure 5 shows four baseline corrected spectral grids of the central 9 × 9 rows and columns within the VOI for volunteer 2. Shown are spectra acquired without motion using ShMoCo, with motion and NoCo, with motion and MoCo, and with motion and ShMoCo. The spectra plotted are the raw spectra after LCModel phase and baseline correction. The spectra with movement and no shim correction had significant baseline distortions.

In a review by Kreis (20) it was recommended that suitable exclusion criteria should include a linewidth threshold between 0.07 and 0.1 ppm and an SNR threshold below the expected range. Figure 6 presents a quality threshold map of the MRSI VOI for each of the scans. Spectra were determined to be within quality bounds if linewidth < 0.08 ppm (9.9 Hz) and $SNR_{LCM} > 7$. Both measures were calculated by LCModel. Alongside the scans with motion is a bar graph showing the magnitude of head rotation (mean of the absolute rotation in up and down positions) for each scan.

A significant increase in the mean linewidth was observed when there was movement and no ShMoCo. The worst case was the motion corrected (MoCo) scan of volunteer 2 with a 9.8 Hz increase (250%) in the mean spectral linewidth, compared to the worst case increase when using ShMoCo of 1.2 Hz (29%) in volunteer 3. The worst mean SNR_{LCM} loss was in the NoCo scan of volunteer 3, whereas the worst case mean SNR_{LCM} loss in the ShMoCo scans was only 13% in volunteer 5.

Figure 7 shows spectral concentration maps for the ratio of NAA to total creatine (tCr) for all the scans. The bar alongside each map demonstrates the magnitude of the movement. Note that LCModel failed to quantify some of the spectra in the uncorrected (NoCo) scan for volunteer 3, these are plotted with zero magnitude.

Agreement between ShMoCo and the baseline scan was analyzed with the statistical method of Bland and Altman (21). Figure 8 shows three Bland-Altman diagrams that plot the differences vs. mean of the NAA to tCr ratio for each of the ShMoCo, MoCo, or NoCo scans relative to the baseline scan (no motion, no correction), respectively. This ratio was chosen because NAA, total NAA, and total creatine were the only metabolites that were consistently quantified to within a 20% SD when no shim correction was employed. In these plots, each of the voxels in the central 5 columns and 7 rows were compared to the corresponding voxels in the baseline scan (stationary with NoCo) for all volunteers. All three had a mean difference of 0.0. The confidence interval with NoCo was −0.45 to 0.44 (31% of mean), with MoCo it was −0.71 to 0.72 (50%), and with ShMoCo it was −0.22 to 0.21 (15%).

The SNR_{NAA} measure was calculated as a quantitative alternative to SNR_{LCM}. In the stationary NoCo scans it was 107, 101, 52, 46, 54, and 64 in volunteers 1 to 6, respectively. Figure 9 shows the effect of motion on the SNR_{NAA} for each of the different scans by plotting the ratio of the mean SNR_{NAA} within the VOI for the relevant scan to the mean SNR_{NAA} of the stationary NoCo scan. This simplifies comparison of the data acquired with two different scanners. The plot demonstrates that for all the scans with motion there was a loss in SNR_{NAA}. The biggest loss in SNR_{NAA} in a ShMoCo scan with motion was 11%, while the biggest loss for non-shim corrected scans with motion was 40% in the same volunteer.

When comparing the three stationary scans that were acquired in volunteer 7 in order to investigate the effect of the vNav on the SNR, the mean SNR_{NAA} across the VOI were 51, 53, and 53, respectively for the standard LASER sequence, the navigated sequence with ShMoCo and the navigated sequence with NoCo. The SNR_{LCM} was 18 for all three scans.

The two motion logs of volunteer 8 who performed pseudo random movements both demonstrated similar patterns of movement with 19 and 20 pose changes in the ShMoCo and NoCo experiments, respectively. No spectra in the ShMoCo scan had observable spectral degradation, while in the NoCo scan several spectra were degraded, particularly the left anterior region of the VOI. The motion log and one spectrum from each scan, voxel 13-13, are plotted in Figure 10. The mean SNR_{LCM} across the VOI were 14, 15, and 12 for the stationary, motion with ShMoCo, and motion with NoCo scans, respectively.

Discussion

Analysis of B0 change with respect to pose

B0 field maps from a single volunteer demonstrate the manner in which head pose affects B0 and thus the mechanism for spectral perturbation. Figure 1 shows the effects of lifting the chin compared to a left-to-right rotation. The chin left-to-right rotations demonstrate an

almost insignificant change in B0 for rotations less than 12°. In the more extreme rotations (magnitude >= 12°) first- and higher-order effects are evident. The otherwise insignificant changes resulting from chin-left-to-right are most likely due to the VOI remaining in a similar region relative to the gradient coordinate system. If the VOI were sagittal or coronal, this probably will reorient accordingly. When rotating the chin up and down, significant frequency changes are evident in each pose. Furthermore, after removing the mean frequency the remaining zero- and higher-order changes demonstrate substantial shifts of up to 20 Hz within the VOI for 10° to 15° rotations.

From the vNav output in our six volunteers who performed a chin-up to -down head rotation, significant mean VOI frequency changes are demonstrated in Figure 4a for rotations with a magnitude greater than 5° The most significant first-order shim change was in the Y (coronal) shim resulting from rotations with a magnitude greater than 3° Figure 4b shows how this Y shim varies almost linearly with angle in the chosen VOI. Small shifts in the Z shim were not consistent between volunteers, however this could be related to differences in their particular motion trajectories.

The second-order shim estimates shown in Figure 4d and e show changes in YZ of up to 5 Hz/cm^2 and in Z^2 of up to 25 Hz/cm^2. To understand the significance of these second-order shims their origin must be pictured at the centre of the MRSI VOI. This can be done as any offset from this origin simply results in the creation of auxiliary zero- and first-order shim terms that have been calculated and analysed independently. In our axial VOI, shim terms incorporating X and/or Y will have the largest range and result in the most significant effect, while a Z dependence will represent a symmetric frequency spread through the slice. Such a frequency spread will tend to produce spectral broadening as a result of negative frequencies below the centre of the slice and positive above. For this reason the YZ shim change will generate a more significant effect than Z^2. For example, at 45 mm away from the centre of an axial slice, a 2 Hz/cm^2 in YZ shim will correspond to a frequency spread through the slice of −6.75 Hz to 6.75 Hz, and across the VOI of −6.75 Hz to 6.75 Hz. As Z and Y are independent the frequency spread through the slice will be linear and proportional line broadening will result. The Z^2 shim demonstrated average changes of 9 Hz/cm^2, however, considering that it only manifests in the slice direction, it results in a parabolic frequency spread across the slice ranging from −5.1 Hz to 5.1 Hz. A parabolic frequency distribution will not be linearly proportional to the resultant line broadening. A single volunteer demonstrated a change in $X^2 - Y^2$ of 0.17 Hz/cm^2, despite its small magnitude the VOI is large in X and Y and will generate a frequency offset at the corner of the VOI of 3 Hz.

Using both the vNav shim estimate logs and the field map model we have demonstrated that both first-order shim and frequency changes in relation to motion are of equal importance. Frequency changes will cause global split peaks. First-order changes will result in position dependent split peaks and line broadening. Second-order changes will generally induce line broadening, but $X^2 - Y^2$ and XY shim changes will also cause split peaks. Therefore, frequency correction alone is not sufficient to maintain spectral quality in the presence of pose changes.

Validation of navigated LASER sequence

The improvement of spectra when using this vNav system in the presence of motion is evident in the spectral plots of Figure 5. Significant spectral and baseline distortions are present in the non-shim-corrected scans with motion - these distortions are markedly reduced when using the vNav. The quality threshold maps of Figure 6 demonstrate that these distortions are consistent across all the volunteers and again show that unlike the non-shim corrected scans, the ShMoCo scans maintained all spectra within the quality bounds, except for a couple of voxels in the frontal lobe of volunteer 4, accounting for 17 % of the VOI.

The Bland-Altman plots of Figure 8 show that in the presence of motion the relative concentration of NAA to tCr remains within a 16% confidence interval.

The lower spectral quality and increased variance in concentration shown in the MoCo scans compared to the NoCo scans likely results from the VOI in the MoCo scans moving relative to the gradient system. Conversely, in the NoCo scans the VOI remains in the same position relative to the gradients but not always in the same anatomical region. Figure 5 demonstrates this behaviour, where the blown up spectra on the right are of good quality in the NoCo scan, but significant split peaks are present in the MoCo scan. It should be noted that the variance in concentration for NoCo scans with movement result from both B0 and anatomical changes.

When using ShMoCo in the presence of motion there was a worst case loss of 13 % in mean SNR and 29 % increase in mean spectral linewidth, which is small in comparison to the values when not using shim correction. It is believed that this loss in spectral quality is the result of second-order and higher B0 inhomogeneities. These changes can be estimated but not corrected on the hardware used.

The stability of the vNav shim estimates is evident in the quality of spectra obtained (Figure 6). Typical frequency and first-order B0 changes are shown in Figure 3b and c with the greatest fluctuations, during stationary periods, occurring in the Z shim at insignificant amplitudes. The reduced stability of shim estimates in Z is due to the small number of vNav data points within the VOI in the slice select direction. The effect of the spectroscopy-specific shim used to acquire the vNav is mitigated by applying real-time first-order shim updates specific to the vNav, potentially also mitigating the effect of susceptibility distortions due to motion.

Figure 3a demonstrates that the vNav in conjunction with PACE is capable of producing precise and reproducible motion estimates. This article has not addressed the benefits of motion correction alone, but rather the combined benefit of motion correction with B0 correction. The lower quality of motion corrected scans compared to uncorrected scans seen in both Figure 6 and Figure 8 does not demonstrate that motion correction reduces the data quality in general, as in this experiment the type of motion used was chosen to emphasise changes in the B0 field.

This work has demonstrated the application of the vNav in an axial slice superior to the ventricles, which is a relatively easy to shim region. When scanning in regions with greater B0 inhomogeneity, such as regions lower down in the brain, it is likely that movement will have a greater effect on B0 perturbation, particularly for left-to-right rotations. In our experience the SNR of the navigator is sufficient to provide stable shim estimates in such regions. However, the navigator FOV may need to be increased in order to cover the intended region.

Although the ability of the vNav to measure second-order changes in B0 homogeneity has been demonstrated, our current hardware does not allow these to be adjusted in real time. The only second-order term the navigator was not able to reliably estimate was Z^2 due to there being only two vNav voxels within the thickness of the VOI (along the Z axis). To reliably fit a second-order term, three data points are needed. This problem may be overcome by increasing the thickness of the chosen volume over which the shim adjustment is performed.

Least squares regression was used to estimate shims - we have not examined how appropriate this is. For MRSI, this approach may result in an inhomogeneous region being neglected in favour of an improvement in another region. A system that minimises the

maximum off resonance (22) regions may prove beneficial when the region of interest is in an area with high B0 inhomogeneity. A technique such as this should be considered to produce uniform spectral quality throughout the VOI.

The proposed sequence does not address subject motion that may occur between the anatomical localiser and the start of the motion tracking procedure, since the tracking reference is created at the beginning of the MRSI scan. This introduces uncertainty in the VOI location and potentially lipid contamination may result. A solution to this could involve online registration of the tracking vNav volume to a structural image – this would provide confidence in the VOI placement and remove the problems of lipid contamination. Alternatively, a technique such as auto-align (23) can ensure a patient specific reference frame before the start of the MRSI acquisition.

In this work, six volunteers deliberately performed mean rotations ranging from 3° to 10° for 2/3 of the scan and one volunteer performed pseudo random head movements. The range of realistic head movements that may be expected during routine MRSI is not documented. Further understanding of the manner in which various population groups move in the scanner would be beneficial to interpreting the practical use of this technique.

The vNav technique corrects for repetition to repetition changes. It does not, however, address intra repetition effects of motion. This may result in dephasing and residual B0 changes. One approach to mitigate such artefacts is to reacquire FIDs that are likely to contain such artefacts. A method has previously been presented (24) where FID's are reacquired when a pose change is detected between two navigators. In our experience, these dephasing and residual effects are difficult to demonstrate in the LASER sequence and require fast and repeated subject movements. Figure 10 demonstrates no observable loss in spectral quality with the subject performing 20 movements during the scan (every 11 to 12 sec). These movements were not timed to avoid the acquisition window. However, if they were performed at a faster rate it is possible that the temporal resolution of the vNav system will be too low, resulting in spectral artefacts. This is a limitation of this method compared to optical tracking devices that typically have a higher temporal resolution and could potentially detect the rate of motion during the spectroscopy part of the acquisition cycle.

The vNav has no observable effect on the spectral SNR or acquisition time. The 714 ms duration of the vNav enabled a TR of 1.5 s to be retained. In the 7^{th} volunteer there was no degrading in the spectral SNR when the vNav was inserted into the sequence compared to the standard LASER sequence. This corroborates the same finding in a single voxel spectroscopy PRESS sequence (9).

Conclusion

Spectral quality in an axial VOI is significantly affected by B0 inhomogeneities resulting from chin up-to-down head rotations. Significant zero- and first-order inhomogeneities were demonstrated with pose changes, particularly in the Y (coronal) direction. The addition of a vNav to the LASER MRSI sequence required no increase in TR or loss in SNR and provided real-time zero- to first-order B0 and motion correction. We have demonstrated that this vNav mitigates motion and B0-related spectral distortions.

Acknowledgments

Several people have provided valuable assistance in this project, including Thomas Benner, Michael Hamm and Charles Harris. We thank Dr. Marjanska Malgorzata from the Center for Magnetic Resonance Research, University of Minnesota, for help with building the LCModel basis set for the LASER sequence. Resources necessary in the project were provided by the University of Cape Town, the Athinoula A. Martinos Center for Biomedical Imaging,

and the Cape Universities Brain Imaging Centre. This study was supported by the South African Research Chairs Initiative of the Department of Science and Technology and National Research Foundation of South Africa, the University of Cape Town, the Medical Research Council of South Africa, NIH grants R21AA017410, R33DA026104, R21EB008547, R01NS055754, P41RR014075, and The Ellison Medical Foundation.

References

1. Posse S, Cuenod CA, Le Bihan D. Motion Artifact Compensation in ^{1}H Spectroscopic Imaging by Signal Tracking. Journal of Magnetic Resonance Series B. 1993; 102:222–227.
2. Henry PG, van de Moortele PF, Giacomini E, Nauerth A, Bloch G. Field-frequency locked in vivo proton MRS on a whole-body spectrometer. Magnetic Resonance in Medicine. 1999; 42:636–642. [PubMed: 10502751]
3. Thiel T, Czisch M, Elbel GK, Hennig J. Phase coherent averaging in magnetic resonance spectroscopy using interleaved navigator scans: compensation of motion artifacts and magnetic field instabilities. Magnetic Resonance in Medicine. 2002; 47:1077–1082. [PubMed: 12111954]
4. Zaitsev M, Speck O, Hennig J, Büchert M. Single-voxel MRS with prospective motion correction and retrospective frequency correction. NMR in Biomedicine. 2010; 23:325–332. [PubMed: 20101605]
5. Weinhandl JT, Armstrong BSR, Kusik TP, Barrows RT, O'Connor KM. Validation of a single camera three-dimensional motion tracking system. Journal of Biomechanics. 2010; 43:1437–1440. [PubMed: 20207358]
6. van der Kouwe AJW, Benner T, Dale AM. Real-time rigid body motion correction and shimming using cloverleaf navigators. Magnetic Resonance in Medicine. 2006; 56:1019–1032. [PubMed: 17029223]
7. Fu ZW, Wang Y, Grimm RC, Rossman PJ, Felmlee JP, Riederer SJ, Ehman RL. Orbital navigator echoes for motion measurements in magnetic resonance imaging. Magnetic Resonance in Medicine. 1995; 34:746–753. [PubMed: 8544696]
8. Tisdall, MD.; Hess, AT.; van der Kouwe, AJW. *MPRAGE* Using EPI *Navigators* for Prospective *Motion* Correction. Proceedings of the 17th annual meeting of International Society of Magnetic Resonance in Medicine,; Honolulu, Hawai'i, USA. 2009. p. 4656
9. Hess AT, Tisdall MD, Andronesi OC, Meintjes EM, van der Kouwe AJW. Real-time Motion and B0 corrected single voxel spectroscopy using volumetric navigators. Magnetic Resonance in Medicine. 2011 (In Press). 10.1002/mrm.22805
10. White N, Roddey C, Shankaranarayanan A, Han E, Rettmann D, Santos J, Kuperman J, Dale A. PROMO: Real-time prospective motion correction in MRI using image-based tracking. Magnetic Resonance in Medicine. 2010; 63:91–105. [PubMed: 20027635]
11. Andronesi OC, Ramadan S, Ratai EM, Jennings D, Mountford CE, Sorensen AG. Spectroscopic imaging with improved gradient modulated constant adiabaticity pulses on high-field clinical scanners. Journal of Magnetic Resonance. 2010; 203:283–293. [PubMed: 20163975]
12. van der Kouwe AJW, Benner T, Salat DH, Fischl B. Brain morphometry with multiecho MPRAGE. Neuroimage. 2008; 40:559–569. [PubMed: 18242102]
13. Ashburner J. A fast diffeomorphic image registration algorithm. Neuroimage. 2007; 38:95–113. [PubMed: 17761438]
14. Thesen S, Heid O, Mueller E, Schad LR. Prospective acquisition correction for head motion with image-based tracking for real-time fMRI. Magnetic Resonance in Medicine. 2000; 44:457–465. [PubMed: 10975899]
15. Jenkinson M. Fast, automated, N-dimensional phase-unwrapping algorithm. Magnetic resonance in medicine. 2003; 49:193–197. [PubMed: 12509838]
16. Reese TG, Davis TL, Weisskoff RM. Automated shimming at 1.5 T using echo-planar image frequency maps. Journal of Magnetic Resonance Imaging. 1995; 5:739–745. [PubMed: 8748496]
17. Tannús A, Garwood M. Improved performance of frequency-swept pulses using offset-independent adiabaticity. Journal of Magnetic Resonance, Series A. 1996; 120:133–137.
18. Ogg RJ, Kingsley PB, Taylor JS. Wet, a T-1-Insensitive and B-1-Insensitive Water-Suppression Method for in-Vivo Localized H-1-NMR Spectroscopy. Journal of Magnetic Resonance Series B. 1994; 104:1–10. [PubMed: 8025810]

19. Provencher SW. Automatic quantitation of localized in vivo 1H spectra with LCModel. NMR in Biomedicine. 2001; 14:260–264. [PubMed: 11410943]

20. Kreis R. Issues of spectral quality in clinical 1H-magnetic resonance spectroscopy and a gallery of artifacts. NMR in Biomedicine. 2004; 17:361–381. [PubMed: 15468083]

21. Bland JM, Altman DG. Statistical-Methods for Assessing Agreement between 2 Methods of Clinical Measurement. Lancet. 1986:307–310. [PubMed: 2868172]

22. Lee J, Lustig M, Kim D, Pauly JM. Improved shim method based on the minimization of the maximum off-resonance frequency for balanced steady-state free precession (bSSFP). Magnetic Resonance in Medicine. 2009; 61:1500–1506. [PubMed: 19319895]

23. van der Kouwe, AJW.; Gicquel, S.; Chen, G.; Schmitt, F.; Harder, M.; Salat, D.; Sorensen, AG.; Fischl, B.; Dale, A. On-line automatic slice positioning and between-scan correction for brain MR protocols. Proceedings of the 11th Annual Meeting of ISMRM; Toronto, Canada. 2003.

24. Hess, AT.; Andronesi, OC.; Tisdall, MD.; Sorensen, AG.; van der Kouwe, AJW.; Meintjes, EM. Motion artefact correction in spectroscopic imaging using an EPI navigator and reacquisition. Proceedings of the 18th annual meeting of International Society of Magnetic Resonance in Medicine; Stockholm, Sweden. 2010. p. 3308

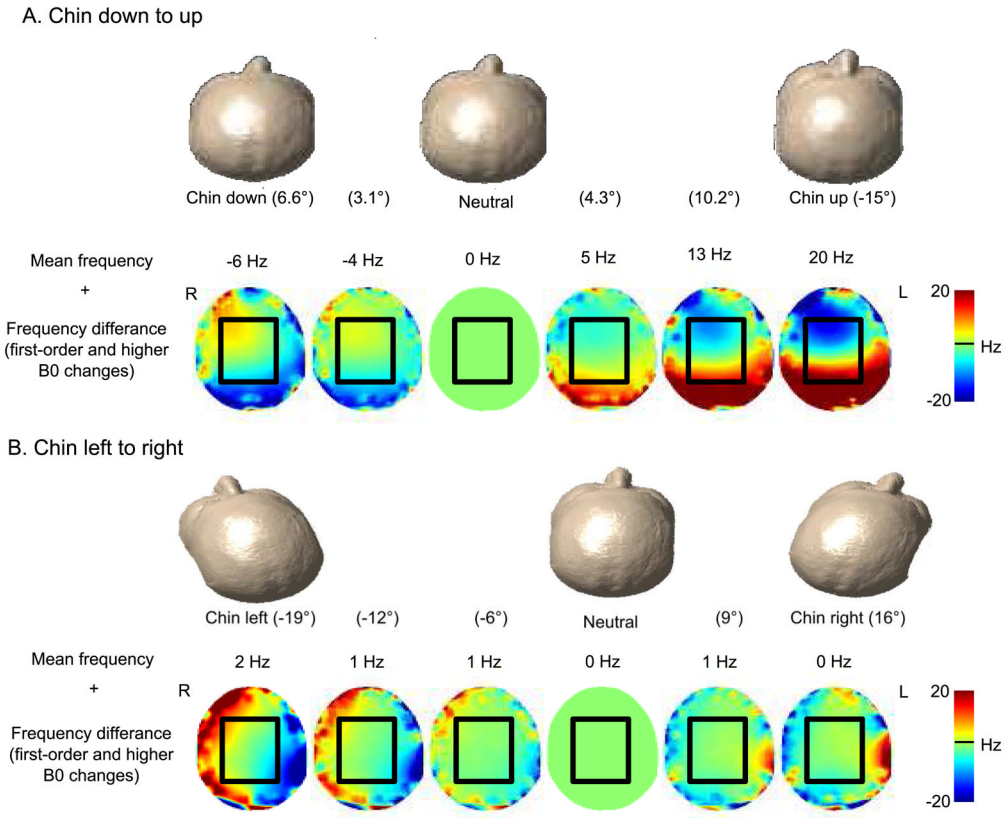

Figure 1.

A 3D reconstruction of the volunteer's head pose, the mean frequency of the VOI in each pose, and the frequency difference (after subtracting the mean, and the frequency map in the neutral pose). The black box is the VOI used. a. Chin-down to -up rotation and b. chin-left to -right rotation.

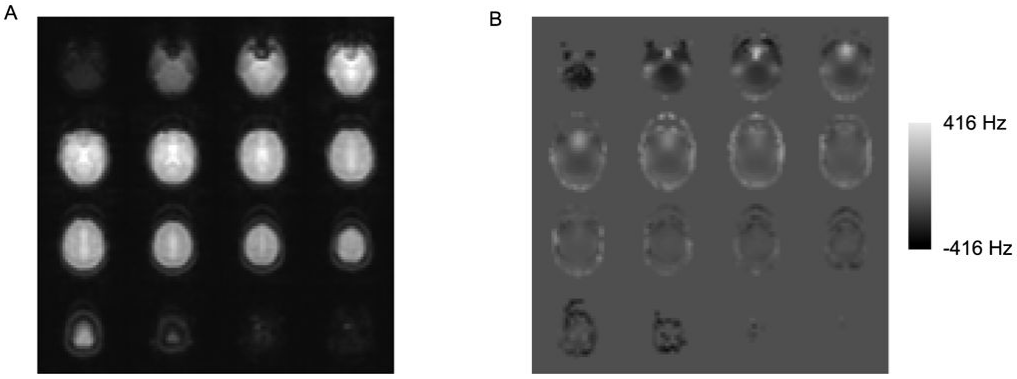

Figure 2.
Example navigator images. A. Magnitude image for first echo, and B. Unwrapped and masked field map with the contrast range doubled (-2π to 2π) due to the phase unwrapping.

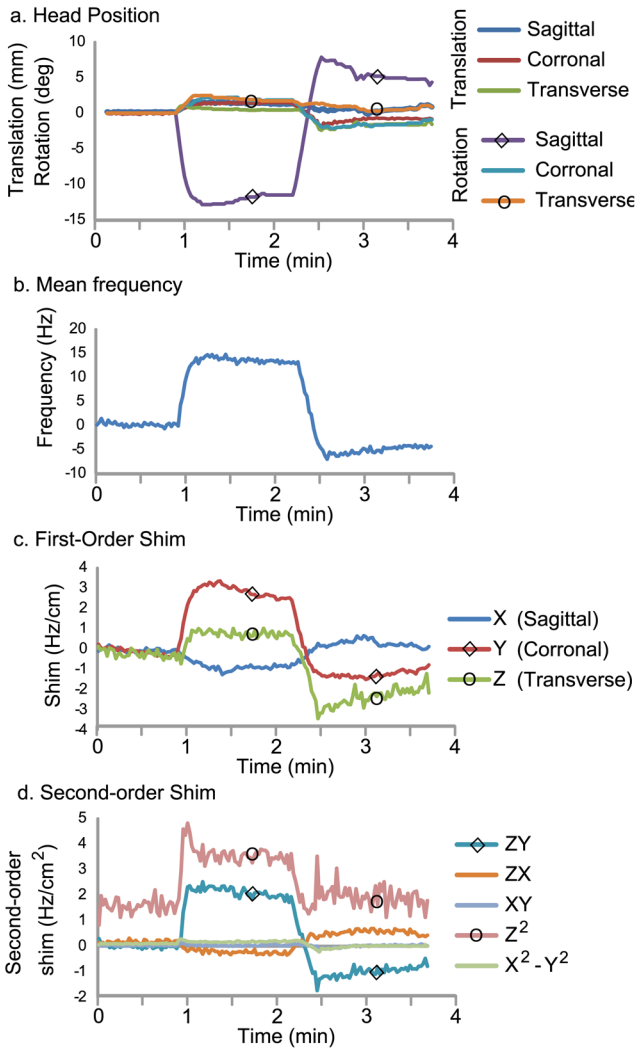

Figure 3.

Motion and shim changes measured by the vNav plotted as a function of time for the ShMoCo scan of volunteer 3. a. Translations and rotations about the scanner's isocenter in scanner XYZ coordinates. b. Changes in mean VOI frequency, measured by the navigator and corrected for real-time first-order gradient changes. C. First-order shim changes within VOI. D. Second-order shim changes measured by vNav.

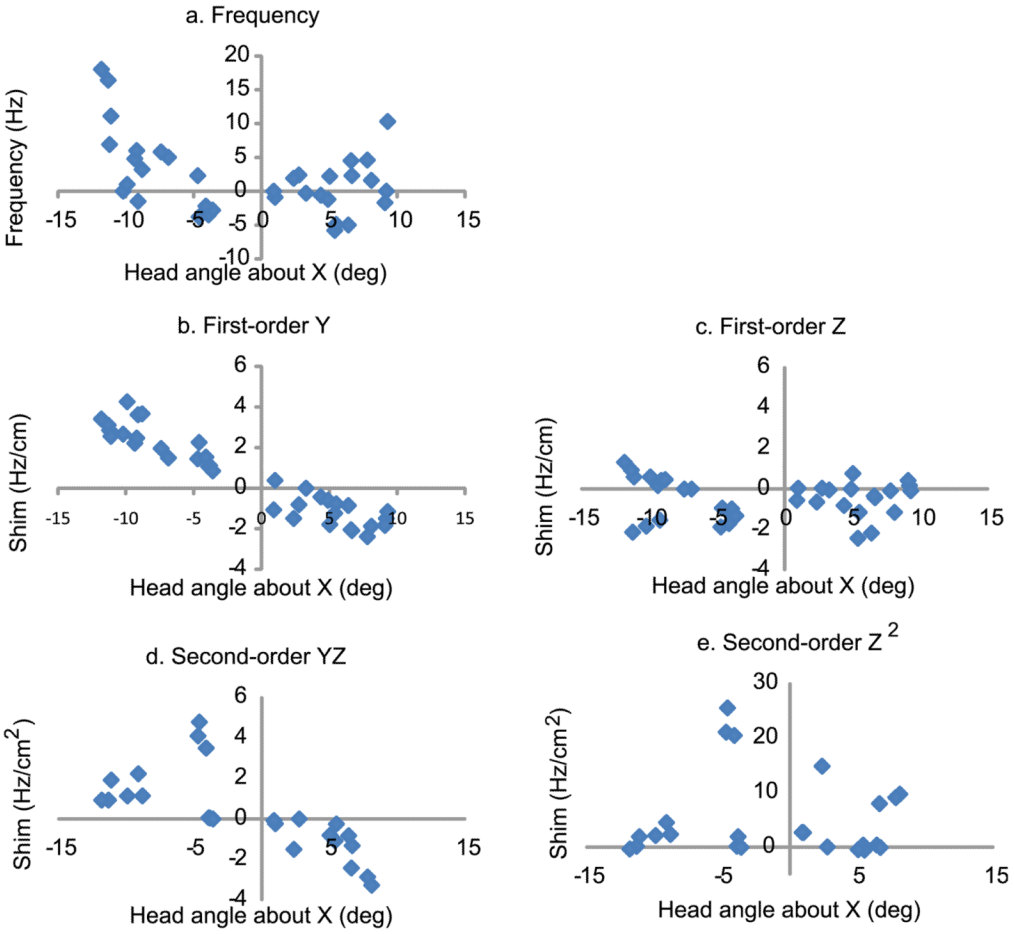

Figure 4.
Shim changes in volunteers as a function of angle of rotation of the head about the X (Sagittal) axis as measured by the vNav. a. Frequency, b. Y (Coronal) shim, c. Z (Transverse) shim, d. YZ second-order shim, and e. Z^2 second-order shim.

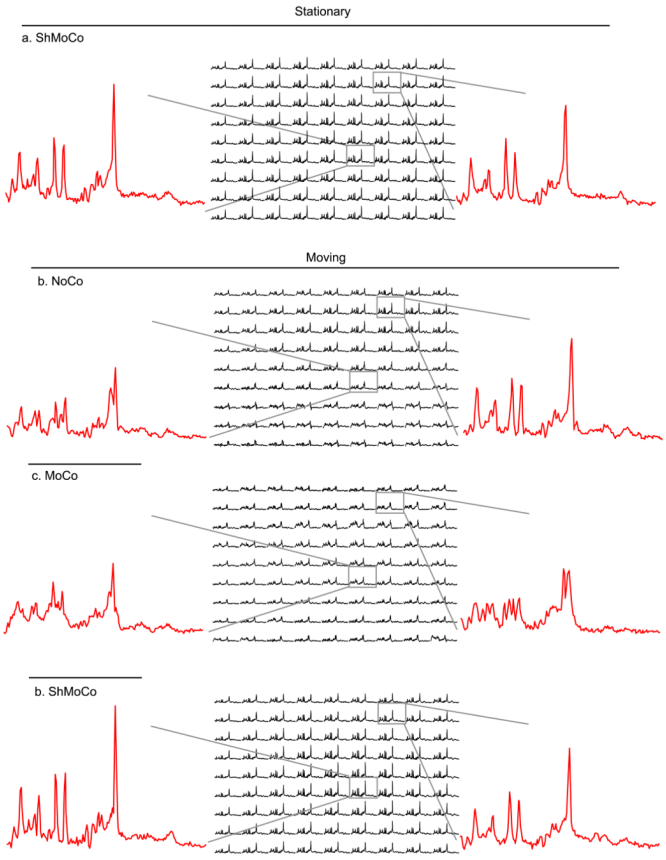

Figure 5.
Spectra for a single volunteer, from the central 9 × 9 rows and columns. a. Stationary Real-time Shim and Motion Corrected (ShMoCo). b. Moving No Correction (NoCo). C. Moving with motion correction (MoCo) but no shim correction. D. Moving with ShMoCo. The spectra shown are the raw spectra after baseline and phase correction in LCModel.

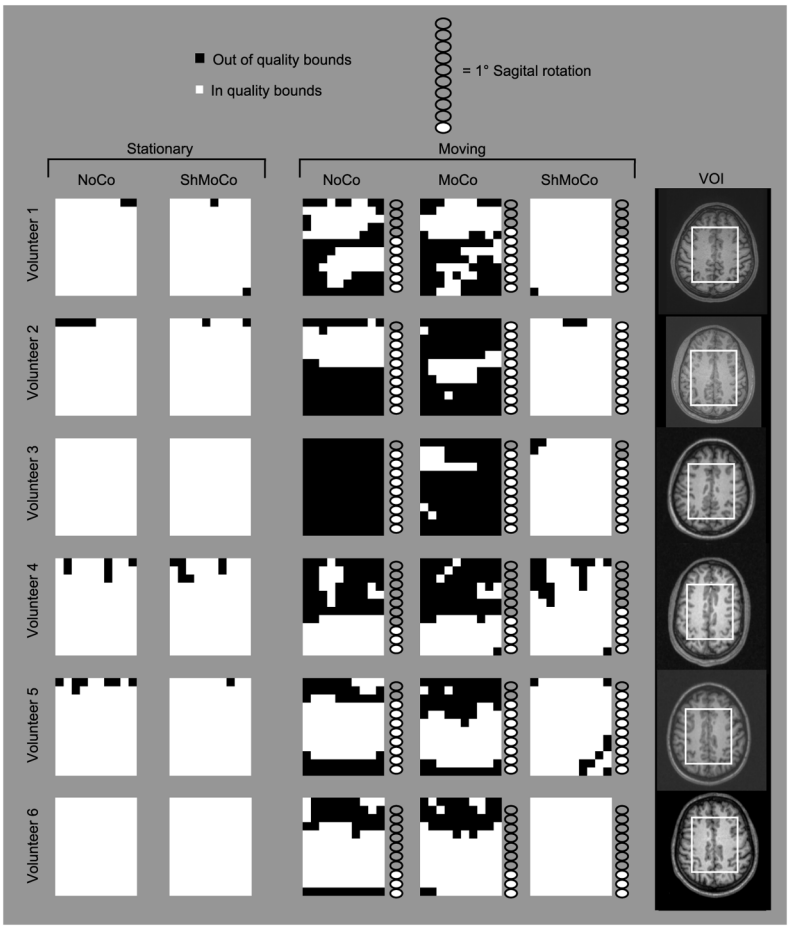

Figure 6.
Map of voxels with acceptable spectral quality (linewidth × 0.08 ppm or 9.9 Hz and SNR × 7) for each scan for each respective volunteer. The scans where the subject moved have a bar graph displaying the mean absolute angle of the chin up and chin down rotation, each bar represents 1° rotation.

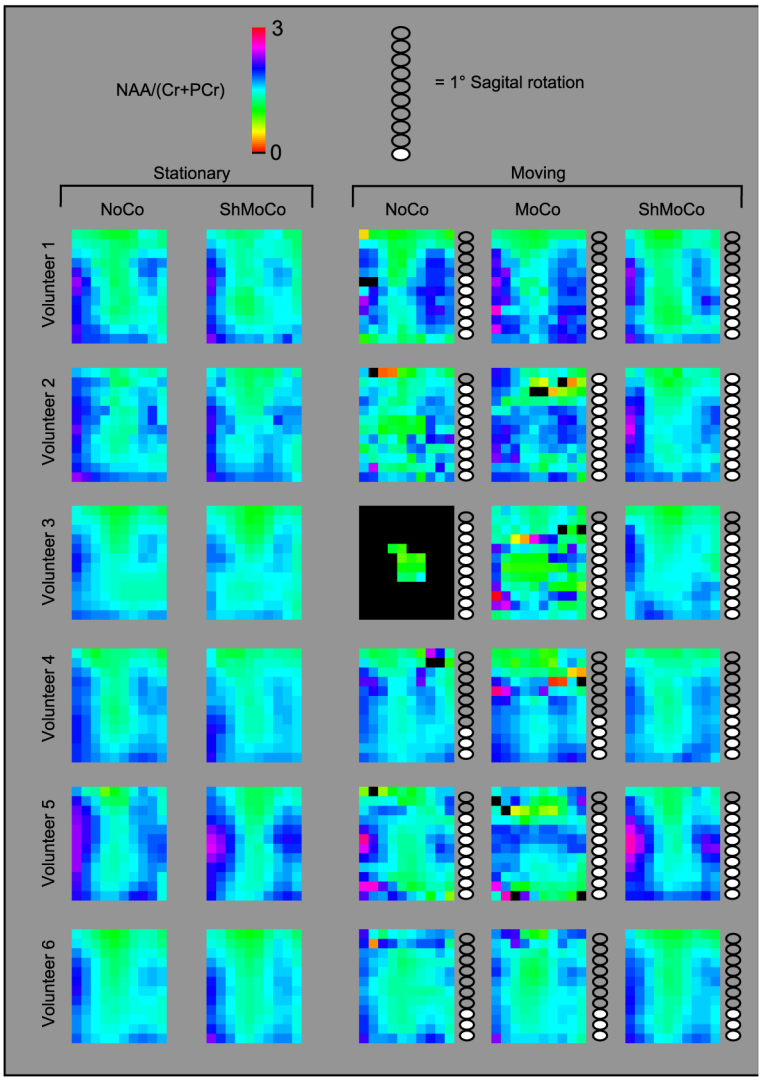

Figure 7.
Map of relative concentration of NAA to total creatine within the VOI for all scans. The bar graph alongside each image with motion indicates the mean absolute angle through which the head was rotated.

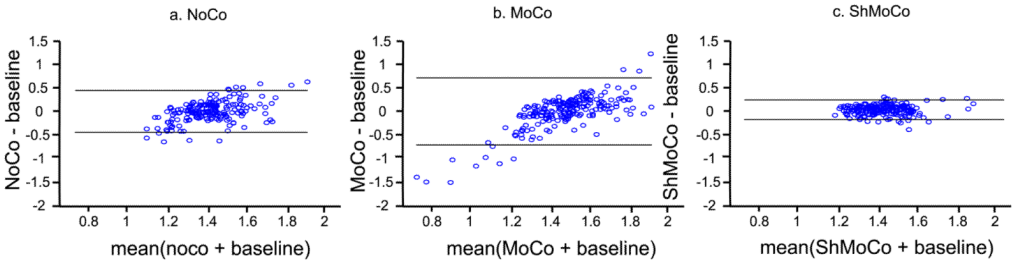

Figure 8.

Bland-Altman plots of the difference vs. mean for the NAA to total creatine for the NoCo, MoCo, or ShMoCo scans relative to the baseline scan (no motion, no correction). a. Scans with motion and no correction (NoCo), b. Motion corrected (MoCo) scans with movement, and c. Real-time shim and motion corrected (ShMoCo) scans with movement.

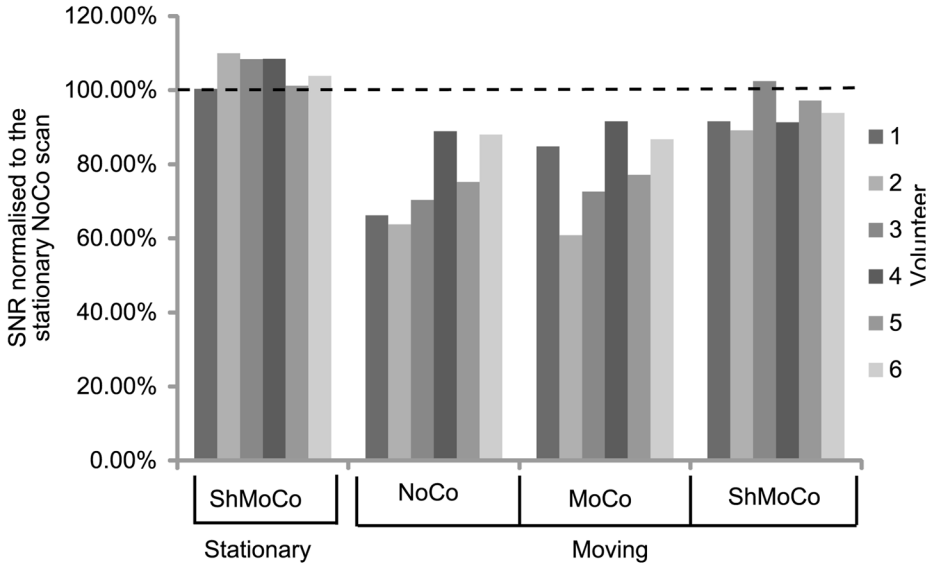

Figure 9.

Effect of motion on the mean SNR_{NAA} within the VOI for each of the different scanning sequences. SNR_{NAA} is the ratio of the NAA maximum and the standard deviation of the signal between 0.5 and 0.2 ppm. Values plotted are the ratio of the SNR_{NAA} for the relevant scan to the SNR_{NAA} in the stationary uncorrected scan.

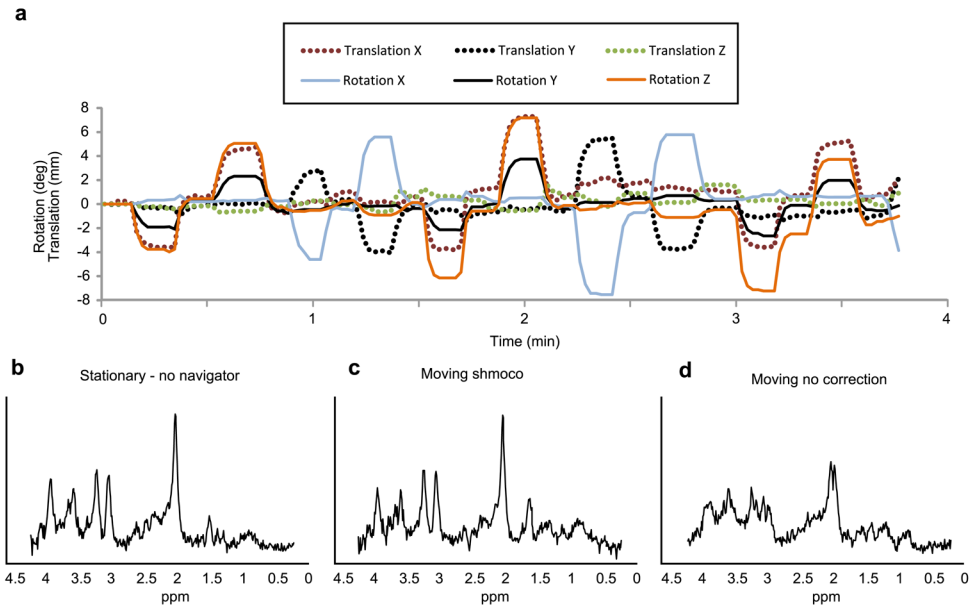

Figure 10.

a) Motion log for scan with pseudo random movements. b) Spectrum for stationary scan with no navigator, c) spectrum for scan with movement, shim and motion correction (ShMoCo), and d) spectrum from scan without any correction applied (NoCo).